J Inorg Organomet Polym (2017) 27:275–284
DOI 10.1007/s10904-016-0470-z

Synthesis and Characterization of Mn_3O_4/BC Nanocomposite and Its Antimicrobial Activity

Bama Krishnan[1] · **Sundrarajan Mahalingam**[1]

Received: 31 August 2016 / Accepted: 12 November 2016 / Published online: 17 November 2016

Abstract Manganese oxide/bentonite clay nanocomposite was synthesized by facile thermal decomposition method, which was characterized by various analysis methods such as X-ray diffraction, fourier transform infra-red spectroscopy, scanning electron microscopy with energy dispersive analysis of X-ray spectroscopy and transmission electron microscopy analysis. Selected area electron diffraction patterns were in good agreement with the XRD results. Antimicrobial studies test were investigated via well-diffusion and potato dextrose agar method, antimicrobial activity of the pristine sodium bentonite clay and prepared sample of Mn_3O_4/BC nanocomposite were reported, against a Gram-negative (*Escherichia coli* and *Pseudomonas aeruginosa*), Gram-positive (*Staphylococcus aureus* and *Bacillus subtilis*) bacterial and fungal (*Candida albicans*) pathogens. The results showed that nanocomposite of Mn_3O_4/BC have enhanced the antimicrobial activity than pristine Na^+–BC.

Graphical Abstract

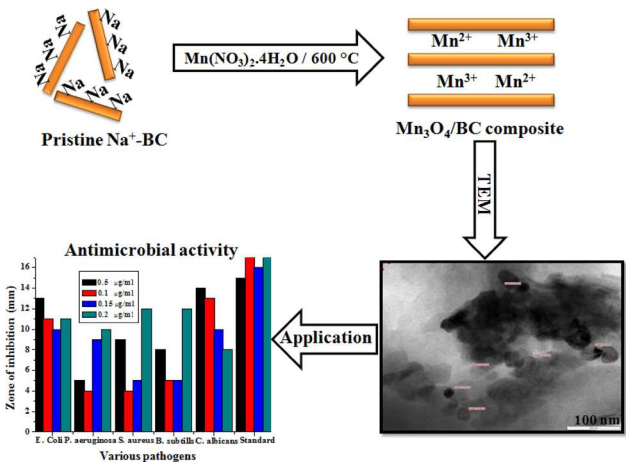

Keywords Sodium bentonite clay · Manganese oxide · Nanocomposite · Nanorods · Antimicrobial activity

1 Introduction

Antimicrobial agents/materials are applied and attracted to many fields in recent years due to the ability to inhibit the growth of micro-organisms. The general methods of synthesized antimicrobial materials are very useful and promising field in research areas like industries [1], food [2], synthetic textiles [3], natural products [4], hospitals, home hygienic, and environmental places [5]. For the past few years, inorganic antimicrobial agents have been used in many fields such as fibers, ceramics, building materials, coating, and enamel, due to their non-toxicity, bio-activity, bio-compatibility, bio-degradability, long life, thermal resistance, and chemical stability compared with organic

Electronic supplementary material The online version of this article (doi:10.1007/s10904-016-0470-z) contains supplementary material, which is available to authorized users.

✉ Sundrarajan Mahalingam
drmsgreenchemistrylab@gmail.com

[1] Advanced Green Chemistry Lab, Department of Industrial Chemistry, School of Chemical Sciences, Alagappa University, Karaikudi, Tamil Nadu 630 003, India

antimicrobial agents. The key advantages of inorganic antimicrobial agents have attracted interest for the control of microbes and improved safety and stability [6]. Inorganic antimicrobial agents are enhanced by adding metal/metal oxide with various inorganic carriers such as kaolinite [7], montmorillonite (MMT) [8], palygorskite (PGS) [6], smectite [9], hectorite [10], bentonite [11], vermiculite [12], sepiolite [13], chitosan [14], starch [15], and zeolite [16].

Among these carriers, low-grade bentonite, especially in sodium form is excellent filler, binder, intercalation, swelling, eco-friendly supporting materials, and substrates for metal/metal oxide composites. Sodium bentonite is a most effective 2:1 layered phyllosilicate type with negative charge, due to the isomorphic substitutions in its structure, which is balanced by the exchangeable cations such as K^+, Na^+, Ca^{2+}, NH^{4+} and Mg^{2+} present in the interlayered spaces. It consists two tetrahedral layers of Si^{4+} ions surrounding by a sandwiched central octahedral layer of Al^{3+} ions, resulting in both strong electrostatic and hydrogen bonding forces. An intercalation of metal oxide into bentonite clay (BC) is one of the important method for modifying the properties of the clay and used for biological applications [17, 18]. In some reports, a modified Ag/BC, Ag/ZnO/Chitosan/BC, Ag/ZnO/BC composites synthesized at room temperature [19] and microwave assisted method [20, 21] without special conditions. In the recent years, several investigations have been focused on intercalated material like metal/metal oxide using bentonite clay such as Ag [22], Cu [23], Ag/Cu [24], TiO_2 [7], Ag/TiO_2 [8], ZnO [6], and MnO_2 [25]. Among these manganese oxide is one of the interesting material, because of their potential applications in diverse areas. Interestingly, manganese oxide intercalated bentonite showed promising antimicrobial effect of the clay that act as single antimicrobial carrier.

Manganese oxide (Mn_3O_4) is one of the most stable oxides. It has attractive physical, chemical properties and wide range of applications in super capacitors [26], catalytic [27], magnetic [28], ion-exchange [29], antibacterial [30], and adsorption properties [31]. Therefore, many of the synthesis approaches such as sol–gel, co-precipitation, wet-chemical, spray pyrolysis, microwave, thermal decomposition, and hydrothermal method have been used to prepare the Mn_3O_4 nanoparticles. Among these methods, thermal decomposition method is one of the promising methods. Using this method, the crystal grains can be developed completely, effectively, simple process, particle size is even disturb and economic method [32]. Mn_3O_4 nanoparticles have been chosen in this work because of its low cost, modest synthesis, environmental benignity and excellent biological performance. This hybrid material is an interesting material due to extensive applications in various areas, such as composite film, polymer matrix, wound dressing material and biological applications [33].

In this paper, we have presented a detailed investigation of Mn_3O_4 intercalated BC nanocomposite synthesized by simple thermal decomposition method. The bactericidal activity of Mn_3O_4 nanoparticles with bentonite was examined against (*Escherichia coli* and *Pseudomonas aeruginosa*), Gram-positive (*Staphylococcus aureus* and *Bacillus subtilis*) bacterial and fungal (*Candida albicans*) pathogens via well-diffusion and potato dextrose agar method. These bacteria and fungi are very sensitive to various environmental pollutants and could be used as good indicators of toxicity. Antimicrobial activity of the pristine sodium bentonite clay (Na^+–BC) and prepared samples of Mn_3O_4/BC nanocomposite also reported.

2 Experimental

2.1 Materials

The sodium bentonite clay (Na^+–BC) was purchased from Merck, India Pvt. Ltd., and it was used as a host material. Manganese nitrate tetrahydrate ($Mn(NO_3)_2{\cdot}4H_2O$) (98%) is used as precursor as well as guest material and sodium hydroxide (NaOH) acting as a precipitating agent. All chemicals were purchased from Sigma-Aldrich Chemicals Pvt. Ltd. All chemicals were used as received without further purification and all the solutions were prepared using de-ionized (DI) water.

2.2 Methods

2.2.1 Synthesis of Manganese (II, III) oxide—Mn_3O_4 (C)

Typically, 0.1 M of manganese nitrate was dissolved in DI water (100 ml). 0.1 M sodium hydroxide was added drop-by-drop into the solution under constant stirring for 3 h at room temperature. After completed the reaction, the resulting homogeneous suspension was allowed to settle at room temperature for 24 h. The obtained black precipitate was centrifuged and washed repeatedly with DI water to remove unreacted chemicals during synthesis process. The sample was dried in an oven at 100 °C for 10 h and ensuing calcinated in muffle furnace at 600 °C for 5 h to obtain Mn_3O_4. The obtained Mn_3O_4 was grinded by mortar and pestle. After grinding, the fine powders of Mn_3O_4 nanoparticles were prepared.

2.2.2 Synthesis of Mn_3O_4/BC Nanocomposite (C_1)

For the synthesized Mn_3O_4/BC nanocomposite, the sodium bentonite clay (10 g) and manganese nitrate tetrahydrate (4.57 g) were dissolved in 100 ml of DI water. The homogenous solid suspension was obtained with the pH 7.

Suspensions were stirred for 3 h at room temperature. The resultant solid suspensions were settled down after 24 h and washed several times with DI water to remove unwanted Na^+ and NO_3^{2-} ions by cationic exchange capacity (CEC) process. The resulting pure solid residue was filtered and dried at 100 °C in an oven for 12 h. The dried sample was calcinated at 600 °C for 5 h and the obtained Mn_3O_4 was grinded by mortar and pestle. Finally the crystalline black powders of Mn_3O_4/BC composite were obtained.

2.3 Characterization

The crystal phases of the nanocomposites were recorded via an X-ray diffraction (XRD) using JEOL (IDX 8030 X'PERT-PRO) instrument operating with Cu-Kα (λ = 1.5418 Å) under the conditions of 40 kV with the current of 30 mA. The functional groups were detected with fourier transform infrared spectroscopy (FT-IR) shimadzu (model-400) using KBr discs in the spectral range of 4000–400 cm^{-1}. The morphology and elemental analysis were studied using scanning electron microscope (SEM with EDX) with working at a 20 kV accelerating voltage. Transmission electron microscope (TEM) (model PHILIPS-CM200) was performed at an accelerating voltage of 20–200 kv, with the resolution 2.4 Å. The samples for TEM analysis were prepared by dispersing the pristine Na^+–BC and Mn_3O_4/BC composite in water by sonicated for 15 min and then drying on a copper grind coated with holey carbon film.

2.4 Antimicrobial Assessment

2.4.1 Optical Density Method

In this study, *E. coli* (ATCC-23848), *P. aeruginosa* (ATCC-27853), *S. aureus* (ATCC-25923) *B. subtilis* (ATCC-11774), and *C. albicans* (ATCC-14053) were used to evaluate the antimicrobial activity test. Pristine Na^+–BC and Mn_3O_4/BC nanocomposite were tested against different pathogens by the well-diffusion and potato dextrose agar method. Pathogenic microorganism culture was prepared by making a phosphate-buffer saline (PBS) suspension of isolated colonies from the 18–24 h of trypticase soy broth (TSB) and cultured overnight at 37 °C in sterile condition. Centrifuge was done at 250 rpm to re-suspend the pathogens and diluted further to form a cell suspension with optical density at 600 nm using UV–Visible spectrophotometer. Stock solution was prepared by taking 1 mL aliquot of cultures in 15% glycol v/v in PSB and stored at −20 °C.

2.4.2 Bactericidal Experiments

In brief, 0.2 µg/ml (microgram/milliliter) of pristine Na^+–BC and various concentrations (0.5, 0.1, 0.15 and 0.2 µg/ml) of synthesized Mn_3O_4/BC nanocomposite was dissolved in dimethyl sulfoxide (DMSO); this suspension was dropped on sterile antibiotic disc and allowed it to dry. Then, the discs were placed on the agar and incubated at 37 °C for 24 h. All fungal isolates were cultured on potato dextrose agar (PDA) medium and adjusted to pH 5.6 at 25 °C. The acidified medium, heated in the acid state hydrolyzed the agar. The same suspension was placed to spread on the PDA for the growth of fungal colonies in a sterile dish. A clear zone of inhibition was observed after 24 h. Amikacin for bacteria, Ketokonazole for fungal and DMSO alone was used as a standard and negative control respectively to compare the antimicrobial behaviour which allows solidifying. The inoculated plates were incubated at 25 °C (aerobic atmosphere) for 3 days. The antimicrobial activities were performed in triplicate.

3 Results and Discussion

The crystal structure of sodium bentonite clay consists of three layers of minerals, in which two tetrahedral (T) and the central octahedral (O) layers (TOT—2:1). The layered sodium aluminosilicate clay was mixed with manganese

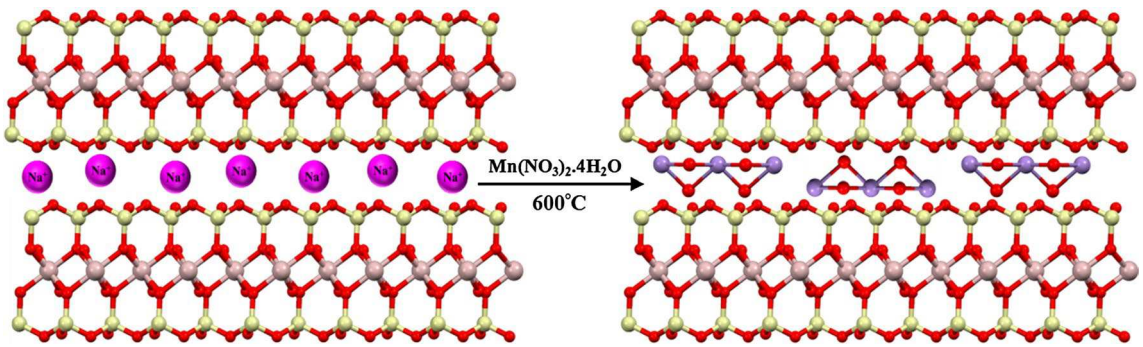

Fig. 1 Schematic illustration for the formation of Mn_3O_4/BC nanocomposite via a thermal decomposition method

precursors in a DI water medium to first initiate the cation exchange process (the existing sodium ions were replaced by the manganese ions). Since the reaction was performed in aqueous medium the as exchanged manganese ions were converted into corresponding hydroxides. Upon successive calcination process at 600 °C, the intermediate compound manganese hydroxide was converted to the Mn_3O_4 [31, 34]. We believe that the ion exchange process was first initiated inside the layers of sodium bentonite. Therefore, the as formed Mn_3O_4 intercalation also possible within the layered structure. Apart from that our surface morphological images reveals that some of the Mn_3O_4 were also formed on the surface of the sodium bentonite clay which confirm that the as formed product is a Mn_3O_4/BC nanocomposite in addition to the manganese oxide intercalation process. The schematic illustration of synthesis process is shown in Fig. 1.

$$Na^+ - BC + Mn(NO_3)_2 + nH_2O \xrightarrow[(H_2O\,medium)]{} Mn(OH)_2 - BC \downarrow + Na^+ + NO_3^{(2-)} + nH_2O \quad (1)$$

$$Mn(OH)_2 - BC + nH_2O \xrightarrow{\Delta} Mn_3O_4/BC + nH_2O \quad (2)$$

4 X-Ray Diffraction Analysis

Figure 2 illustrates the XRD pattern of pristine Na^+–BC, Mn_3O_4, and the Mn_3O_4/BC composite. The XRD patterns of the pristine Na^+–BC was observed at 2θ values 19.7°, 34.9°, 54.4°, 61.9°, and 73.5° and it corresponds to the crystallographic planes of (101), (107), (013), (011), and (308) and the peaks are evident in all patterns, which are also consistent with other previous works [21] (these peaks are indicated by B in Fig. 2a). The XRD patterns of the Mn_3O_4 nanoparticles are shown in Fig. 2b. All the diffraction peaks at 2θ values 18.2°, 28.9°, 32.4°, 36.2°, 45.4°, 53.6°, 56.2°, 58.4°, and 63.1° corresponds to different lattice planes of (101), (112), (103), (211), (213), (312), (303), (321), and (116) as the tetrahedral structures (body centered cubic-BCC) are quite matching with the JCPDS card No. 89-4837 (these peaks are indicated by M in Fig. 2b) [31]. After Mn_3O_4 nanoparticles intercalated into BC surface, new peaks are observed corresponding to the formation of Mn_3O_4/BC composite. These new peaks were reflected at 2θ = 19.8°, 20.9°, 28.0°, and 36.5° for Mn_3O_4 and also peak intensity and crystallinity of BC have decreased, most probably due to the presence of Mn_3O_4 in BC (these peaks are indicated by B and M in Fig. 2c). The additional peaks were observed with various intensities for Mn_3O_4 intercalated BC and compared with pristine Na^+–BC as shown in Fig. 2 [34]. The average crystalline size can be calculated from Debye Scherrer formula.

$$D = 0.89\lambda/\beta\cos\theta \quad (3)$$

The calculated D values of Mn_3O_4 and Mn_3O_4/BC composite expected around 25 and 11 nanometer (nm). The sharp peaks were clearly indicating that the formation of Mn_3O_4/BC composite with smaller crystalline size at 600 °C than the Mn_3O_4 nanoparticles.

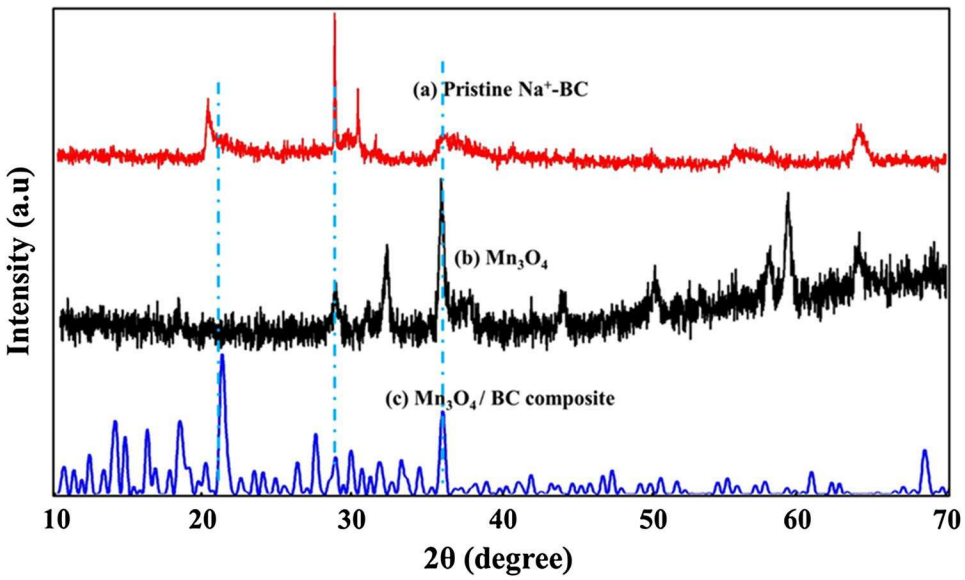

Fig. 2 XRD diffraction patterns for **a** pristine Na^+–BC, **b** Mn_3O_4 nanoparticles, and **c** Mn_3O_4/BC composite

Table 1 Comparison FT-IR spectrum values of pristine Na^+–BC, Mn_3O_4 nanoparticles and Mn_3O_4/BC nanocomposite

Pristine Na^+–BC (cm^{-1})	C (cm^{-1})	C_1 (cm^1)	Functional group
3637	3426	3613	–O–H groups stretching [35]
3415	–	3400	
2803	–	2779	H–O–H bending and the hindered rotation of water molecules [35]
1701	–	1649	–OH deformation of H_2O [35]
1035	–	1043	Si–O and Si–O–Si stretching in T_d sheet [21]
619	608	607	Si–O and Al–O out-of-plane, Mn–O stretching (tetrahedral sites) [27, 31, 35]
527	500	527	Si–O–Al bending and stretching vibrations and Mn–O (octahedral sites) [27, 31, 35]
466	–	470	Si–O–Si bending vibration [21]

Na^+–BC sodium bentonite clay, *C* Mn_3O_4 nanoparticles, *C_1* Mn_3O_4/BC composite]

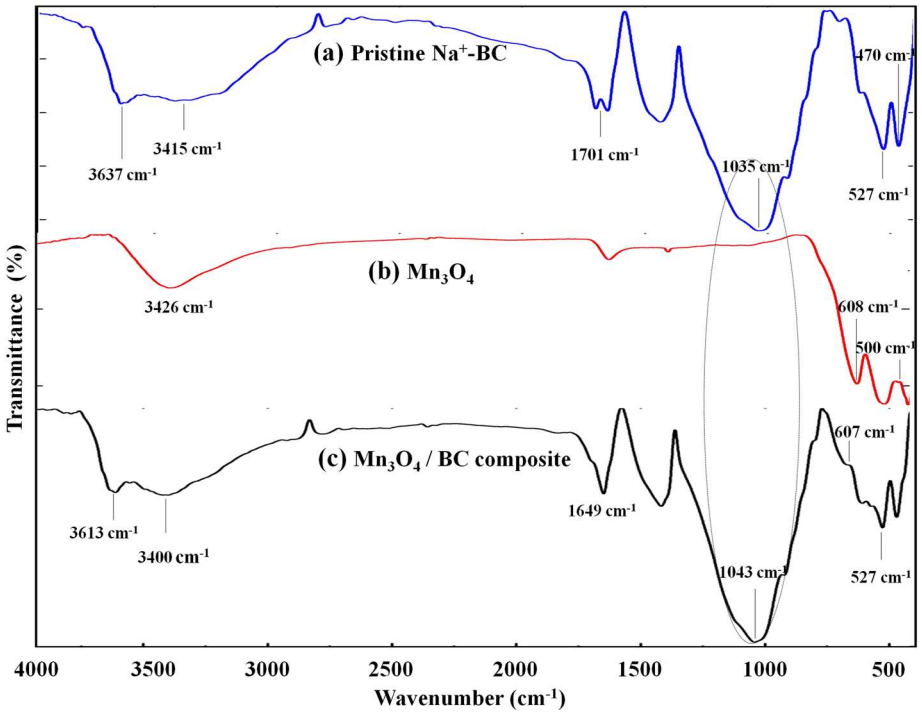

Fig. 3 FT-IR patterns of **a** pristine Na^+–BC, **b** Mn_3O_4 nanoparticles, and **c** Mn_3O_4/BC composite

4.1 FT-IR Analysis

Figure 3 shows a comparison of FT-IR spectrum for pristine Na^+–BC, Mn_3O_4 nanoparticles, and Mn_3O_4/BC composite in the range of 4000–400 cm^{-1} and the corresponding assignments are given in Table 1. Figure 3a shows the vibration bands at 3637 and 3415 cm^{-1} arises due to interlayered O–H stretching [35]. The peak observed at 2803 cm^{-1} is attributed to the aliphatic hydrocarbons ignition in Na^+–BC. A small narrow band at 1653 cm^{-1} has been attributed –OH group of angular and deformation of H_2O hydration [35]. The peaks assigned to Si–O and Si–O–Si stretching in tetrahedral sheet at 1035 and 920 cm^{-1} are indicates to reflect the stretching vibration of A1–O–OH–Al and Al–Al–OH respectively [21]. Besides, peak at 707 cm^{-1} is corresponded to Si–O and Al–O out-of-plane and platy form of quartz admixture in the Na^+–BC sample which has been confirmed by XRD pattern. The small peaks at 619 and 527 cm^{-1} were observed to the Si–O, Si–O–Si and Al–O–Si bending vibration [35]. A sharp peak at 466 cm^{-1} should be ascribed to the Si–O–Si in this pristine Na^+–BC [21]. These results are consistent with previous works [20, 21]. Figure 3b shows the three main absorption peaks at 3426 cm^{-1} is attributed to O–H stretching and bending modes of adsorbed water. The peaks at 608 and 500 cm^{-1} are assigned with the coupling between Mn-O stretching modes of tetrahedral A (Mn^{2+}) and octahedral B (Mn^{3+}) sites as normal spinel structure, which were reported in the literature on Mn_3O_4 nanoparticles [25, 27, 35].

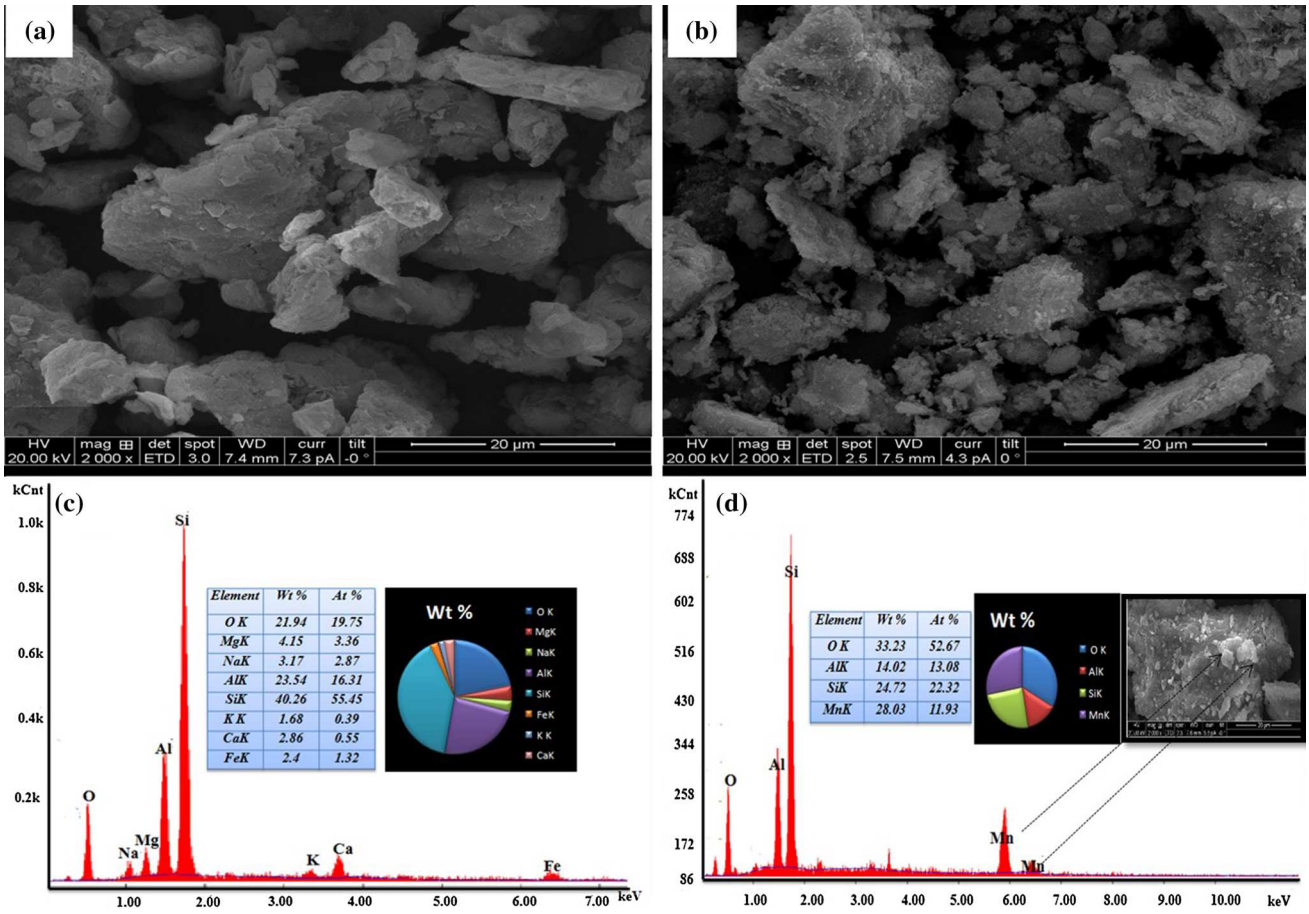

Fig. 4 SEM images with of pristine Na^+–BC **a** and Mn_3O_4/BC composite **b** and the corresponding energy dispersive X-ray spectroscopy images shown in (**c**) and (**d**), respectively. The nanoparticles of Mn_3O_4 shown in inserted image of (**d**) with *arrows*

Figure 3c shows all peaks in Mn_3O_4/BC composite samples shift to lower wave numbers and decreased peak intensity were associated with O–H and Al–OH. The peak at 1701 cm^{-1} was slightly changes, during intercalation process. The new peaks at 607 and 527 cm^{-1} were observed after the intercalation of the Mn_3O_4 nanoparticles into the BC and these peaks due to the tetrahedral and octahedral phase of Mn–O bond. This spectrum concluded that the major changes occurred in Mn_3O_4/BC composite layers and on the surfaces, due to the interaction Mn_3O_4 nanoparticles. This result confirmed that the Mn_3O_4 nanoparticles present in the BC [34].

4.2 SEM Analysis

Figure 4 shows the SEM images of pristine Na^+–BC and Mn_3O_4/BC composite and it is appeared different morphologies at the same magnification. The SEM image of Na^+–BC showed clearly visible flat structure, irregular platelets form and coarse morphology is shown in Fig. 4a [36]. Figure 4b shows SEM image of the Mn_3O_4/BC composite. After modification with Mn_3O_4 nanoparticles, the BC surface was completely changed with few aggregates, irregular small spherical particles and separated flakes on the BC surface. This might be due to the electrostatic attraction in between the interlayers cations and host material of BC surface [37].

4.3 Energy Dispersive X-Ray Spectroscopy

The synthesized composite material was also characterized by EDX, and the results are shown in Fig. 4c, d. The EDX spectrum of pristine Na^+-BC are shown in Fig. 4c, which indicates the presence of Si, Al, O and Na. An element of Mn and O are presented in Fig. 4d, which confirms that the intercalated manganese and oxygen into BC due to the lower isomorphic substitution and exchangeable interlayer cation.

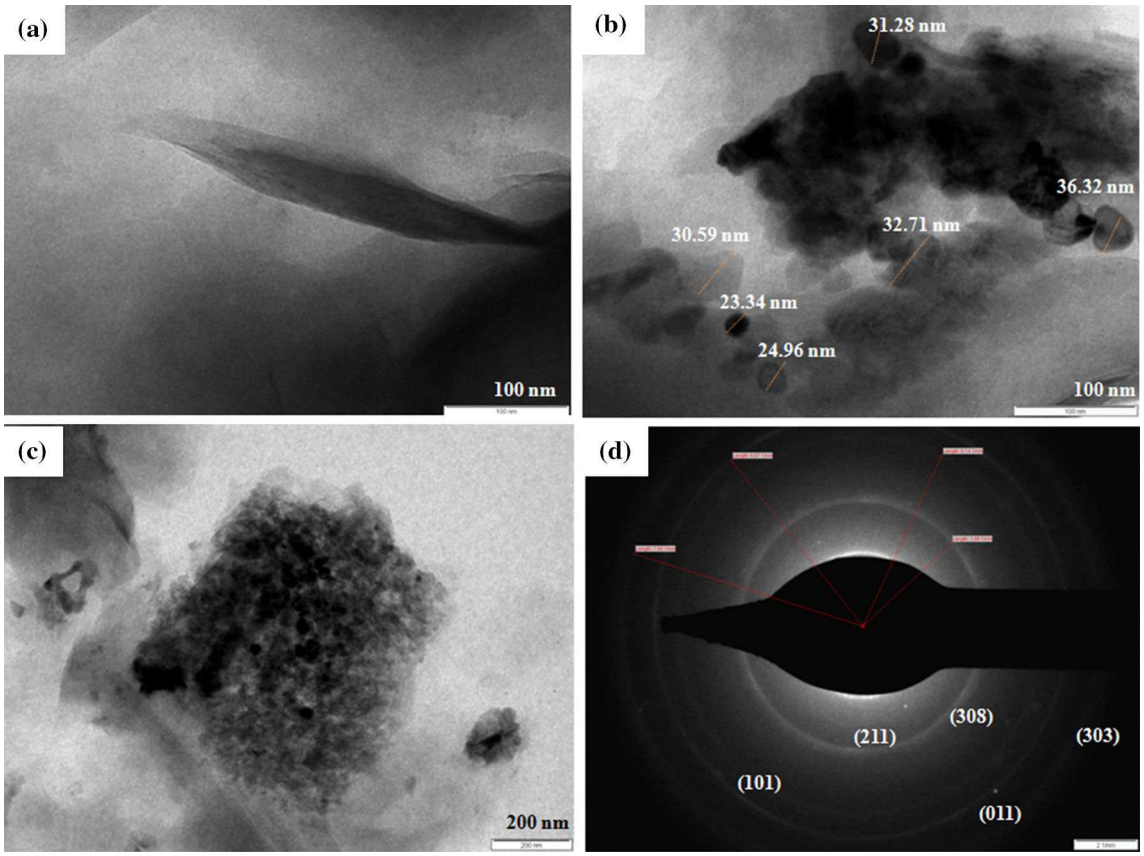

Fig. 5 TEM images pristine Na^+–BC (**a**), Mn_3O_4/BC nanocomposite at different magnifications (**b**) and (**c**) and SAED pattern of Mn_3O_4/BC nanocomposite (**d**). The particles sizes of the Mn_3O_4 were mentioned in **b**

4.4 TEM Analysis

TEM micrographs of pristine Na^+–BC and Mn_3O_4/BC nanocomposite are shown in Fig. 5. A typical TEM image of pristine Na^+–BC sample exists in flat and platelets structure with 100 nm size as shown in Fig. 5a. This observation is consistent with the earlier findings by the other researchers [37].

The exceptional shape and size distribution of the Mn_3O_4/BC composite can be clearly observed in TEM images. The TEM images (Fig. 5b, c) of Mn_3O_4/BC composite have many fine spherical shapes with small sizes. These structures may therefore represent certain material containing Mn_3O_4 nanoparticles, which shown with different magnifications in Fig. 5b, c. Compared with the pristine Na^+–BC the Mn_3O_4/BC nanocomposite surface was noticeably changed. Consequently, the layered structure of BC was not affected, while the Mn_3O_4 nanoparticles intercalated into the surface of BC. In addition, BC shape and surface was entirely changed as shown in Fig. 5a–c. Moreover, the SAED patterns of the Mn_3O_4/BC nanocomposite shown in Fig. 5d indicates the diffraction crystallinity rings and white spots confirms the high degree of crystalline and polycrystalline nature of Mn_3O_4/BC nanocomposite. These patterns indicated the well crystallized Mn_3O_4 in good agreement with the BCC of XRD results and the standard JCPDS card No. 89-4837 were confirmed [6].

Table 2 Zone of inhibition (mm) values of pristine Na^+–BC against different test microorganisms both bacterial and fungal pathogens

Pathogenic names	Zone of inhibition of pristine clay (mm)	Zone of inhibitions of standard sample (mm)
E. coli	8	8
P. aeruginosa	5	9
S. aureus	3	2
B. subtilis	2	10
C. albicans	6	8
Control	R	R

4.5 Antimicrobial Activity

The antimicrobial activity expressed at the zone of inhibition in millimeter (mm). The values of the samples were assessed using bacterial and fungal strains. The

Table 3 Zone of inhibition (mm) values of different concentration of Mn_3O_4/BC nanocomposite against different test microorganisms both bacterial and fungal pathogens

Various pathogens name/ Mn_3O_4/BC nanocomposite different concentration	0.5 (μg/ml)	0.1 (μg/ml)	0.15 (μg/ml)	0.2 (μg/ml)
E. coli	13	11	10	11
P. aeruginosa	5	4	9	10
S. aureus	9	4	5	12
B. subtilis	8	5	5	12
C. albicans	14	13	10	8
Standard	15	17	16	17
Control	R	R	R	R

antimicrobial activities of pristine Na^+–BC and synthesized Mn_3O_4/BC nanocomposite were evaluated against different pathogenic microorganism using standard zone of inhibition (ZOI) assay. The antimicrobial studies of the same samples were tested against *E. coli, P. aeruginosa, S. aureus, B. subtilis* bacteria, *and C. albicans* fungal pathogens were performed by well-diffusion and potato dextrose agar method [28, 38]. The antimicrobial studies results were presented in Tables 2 and 3. In Fig. 6a-d showed that the pristine Na^+–BC (0.2 μg/ml) and Mn_3O_4/BC nanocomposite at various concentrations (0.5, 0.1, 0.15 and 0.2 μg/ml) showed a clear zone of inhibition around each sample, indicating an obvious effect against bacteria. The bacterial effect of nanocomposites depends on the large specific surface area, smaller sizes of the particles, which allow them to interact closely with cell wall membranes.

Zone of inhibition values of Mn_3O_4/BC nanocomposite was larger than the pristine Na^+–BC. DMSO does not have any role in the zone of inhibition and nanocomposite shows the higher zone of inhibition based on the valuable reasons as follows. (i) The differences in microbial activity are caused by structural variations of their cell walls. The Mn_3O_4/BC nanocomposite had relatively high antibacterial activity against gram negative (*E. coli* and *P. aeruginosa*) bacteria as compared to that of gram positive (*S. aureus* and *B. subtilis*) bacteria [38]. (ii) This is due to the presence of primarily thick peptidoglycan layer and teichoic acid in gram positive bacteria whereas in case of gram negative bacteria composed of a lipopolysaccharides phospholipid asymmetric bilayer, mainly peptidoglycan layer is thin and teichoic acid is absent [38]. The absence of teichoic acid in the gram negative bacteria leads to increase the penetrations and might cause membrane damage of nanocomposite to the cell wall. Moreover, the mechanism of antibacterial effect of manganese ions exchanged bentonite have been ascribed to the attraction, through electrostatic forces, rupturing the cell walls, and causing the leakage of cytoplasm on the negatively charged membrane of the bacteria cell wall to BC surface [39]. Overall, Mn_3O_4 nanoparticles can kill some bacteria and BC has slightly antimicrobial activity because both are attached to the bacteria surface.

Mn_3O_4/BC nanocomposite showed an efficient antimicrobial activity against pathogens, due to the important reasons: (i) electrostatic attraction, (ii) nanocomposite reacted with peptidoglycan, teichoic acids, lipoteichoic acid and (iii) cytoplasm membranes inside the cell wall [20] (iv) increase in antimicrobial efficiency with thickness may be due to increased number of manganese, silicon, aluminium and hydroxyl ions released from the Mn_3O_4/BC nanocomposite, which kills the microorganisms [40]. (v) Among these few reasons the structure of bacterial cell wall is damaged easily [21]. Mn_3O_4/BC nanocomposite is the first innovative and development of an efficient antimicrobial application under simple and eco-friendly method [20].

5 Conclusion

We have successfully synthesized Mn_3O_4/BC nanocomposite by facile thermal decomposition method without using any hazardous chemicals. The particle size of the nanocomposite was observed by TEM. The average size of the particles was around 100 and 200 nm. The TEM observations confirmed the nanoparticles with dark area represent Mn_3O_4 on/into the BC surface. Bioactivity of pristine Na^+–BC and Mn_3O_4/BC nanocomposite was demonstrated by studying antimicrobial activity of suspension with various concentrations using standard microbial method. The small particles of nanocomposite was penetrating a pathogenic cell wall which results in the generation of high electrostatic interaction and reactive oxygen species, which will kill microorganism more effectively. Results of antimicrobial test were shown better zone of inhibition of Mn_3O_4/BC nanocomposite compared to pristine Na^+–BC. The results confirmed that the order of antimicrobial activities of Mn_3O_4/BC nanocomposite was higher than pristine Na^+–BC (Mn_3O_4/BC > BC). Finally, Mn_3O_4/BC nanocomposite is promising material for antipathogenic application in environments such as hospitals, schools and common places to keep it clean and healthy.

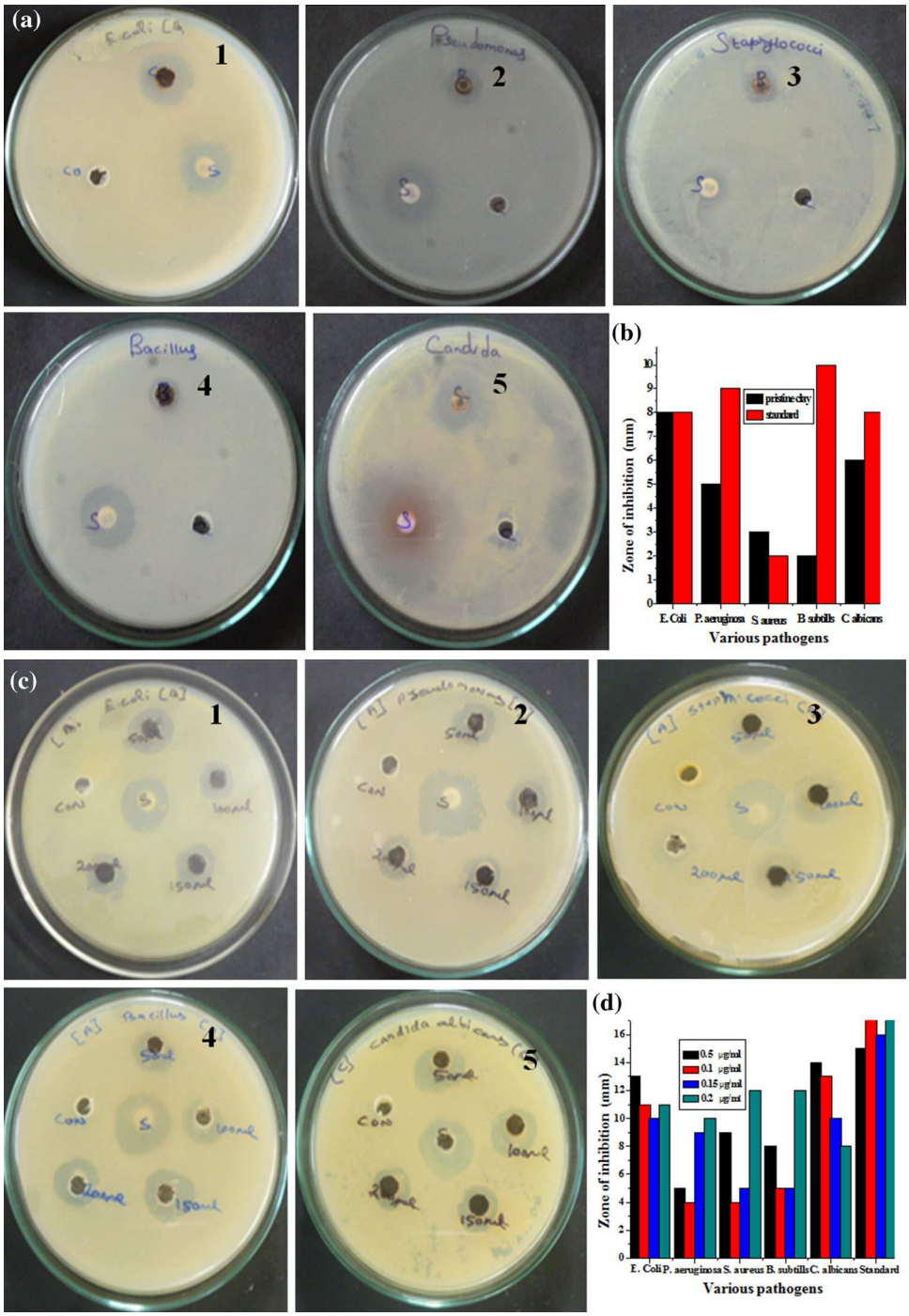

Fig. 6 **a, c** The digital photographs of antimicrobial activities of pristine Na^+–BC and different concentration of Mn_3O_4/BC nanocomposite against different microorganisms like Gram-negative (*E. coli* and *P. aeruginosa)*, Gram-positive *(S. aureus* and *B. subtilis)* bacterial, and fungal *(C. albicans)* and **b, d** zone of inhibition (mm) values of pristine Na^+–BC and different concentration of Mn_3O_4/BC nanocomposite using graphical results. [*E. Coli, Escherichia coli* (1); *P. aeruginosa, Pseudomonas aeruginosa* (2); *S. aureus, Staphylococcus aureus* (3); *B. subtilis, Bacillus subtilis* (4); *and C. albicans, Candida albicans* (5)] respectively

Acknowledgements The authors express their sincere thanks to Professor and Head, Department of Industrial Chemistry and Department of Physics for providing SEM and XRD facilities, Alagappa University, Karaikudi, Tamil Nadu, India.

References

1. H. Zhang, X. Lv, X. Zhang et al., RSC Adv. **5**, 50523 (2015)
2. R. Sothornvit, J.-W. Rhim, S.-I. Hong, J. Food Eng. **91**, 468 (2009)
3. M. Ul-Islam, T. Khan, W.A. Khattak, J.K. Park, Cellulose **20**, 589 (2013)
4. C. Delhom, L. White-Ghoorahoo, S. Pang, Compos. Part B **41**, 475 (2010)
5. T. Corrales, I. Larraza, F. Catalina et al., Biomacromolecules **13**, 4247 (2012)
6. C. Huo, H. Yang, Appl. Clay Sci. **50**, 362 (2010)
7. C. Wang, H. Shi, P. Zhang, Y. Li, Appl. Clay Sci. **53**, 646 (2011)

8. T.-S. Wu, K.-X. Wang, G.-D. Li, S.-Y. Sun, J. Sun, J.-S. Chen, ACS Appl. Mater. interfaces **2**, 544 (2010)
9. S.R. Wasserman, L. Soderholm, U. Staub Chem. Mater. **10**, 559 (1998)
10. I. Fatimah, Int. J. Chem. Sci. **10**, 1341 (2012)
11. F. Tomul, Ind. Eng. Chem. Res. **50**, 7228 (2011)
12. M. Hundakova, M. Valášková, V. Tomášek, E. Pazdziora, K. Matějová, Acta Geodynamica et Geomaterialia **10**, 97
13. A. Esteban-Cubillo, C. Pecharromán, E. Aguilar, J. Santarén, J.S. Moya, J. Mater. Sci. **41**, 5208 (2006)
14. K. Shameli, M.B. Ahmad, W.M.Z.W. Yunus, et al., Int. J. Nanomed. **5**, 875 (2010)
15. K. Shameli, W. Yunus, W.M. Zin, N.A. Ibrahim, M. Darroudi, Aust. J. Basic Appl. Sci. **4**, 2158 (2010)
16. K. Shameli, M.B. Ahmad, M. Zargar, W. Yunus, N.A. Ibrahim, Int. J. Nanomed. 6, 331 (2011)
17. R. Srinivasan, Adv. Mater. Sci. Eng. (2011)
18. J. Liu, G. Zhang, Phys. Chem. Chem. Phys. **16**, 8178 (2014)
19. J.A. Do Rosário, G.B. De Moura, M. Gusatti, H.G. Riella, Chem. Eng. 17, 1017 (2009)
20. S.C. Motshekga, S.S. Ray, M.S. Onyango, M.N. Momba, Appl. Clay Sci. **114**, 330 (2015)
21. S.C. Motshekga, S.S. Ray, M.S. Onyango, M.N. Momba, J Hazard Mater **262**, 439 (2013)
22. S.K. Pillai, S.S. Ray, M. Scriba, J. Bandyopadhyay, M. Roux-van der Merwe, J. Badenhorst, Appl. Clay Sci. **83**, 315 (2013)
23. L. Fu, B.M. Weckhuysen, A. Verberckmoes, R.A. Schoonheydt, Clay Miner. **31**, 491 (1996)
24. M Hundáková, M Valášková, J Seidlerová, Nano con. **16**, 10 (2013)
25. E. Eren, B. Afsin, Y. Onal, J. Hazard. Mater. **161**, 677 (2009)
26. L.L. Zhang, T. Wei, W. Wang, X. Zhao, Microporous Mesoporous Mater. **123**, 260 (2009)
27. X. Li, L. Zhou, J. Gao, H. Miao, H. Zhang, J. Xu, Powder Technol. **190**, 324 (2009)
28. T. Ozkaya, A. Baykal, H. Kavas, Y. Köseoğlu, M.S. Toprak, Phys. B **403**, 3760 (2008)
29. H. Xia, Y. Wang, J. Lin, L. Lu, Nanoscale Res. Lett. **7**, 1 (2012)
30. A.-N. Chowdhury, M.S. Azam, M. Aktaruzzaman, A. Rahim, J. Hazard. Mater. **172**, 1229 (2009)
31. Z. Durmus, H. Kavas, A. Baykal, M. Toprak, Open. Chem. **7**, 555 (2009)
32. Z. Durmus, M. Tomas, A. Baykal, H. Kavas, T.G. Altınçekiç, M.S. Toprak, Russ. J. Inorg. Chem. **55**, 1947 (2010)
33. E. Abdullayev, K. Sakakibara, K. Okamoto, W. Wei, K. Ariga, Y. Lvov, ACS App. Mater. Interfaces **3**, 4040 (2011)
34. S. Sohrabnezhad, M.M. Moghaddam, T. Salavatiyan, Spectrochim. Acta Part A Mol. Biomol. Spectrosc. **125**, 73 (2014)
35. L. Zhirong, M.A. Uddin, S. Zhanxue, Spectrochim. Acta Part A Mol. Biomol. Spectrosc. **79**, 1013 (2011)
36. J. Hua, Appl. Clay Sci. **114**, 239 (2015)
37. C. Yang, Y. Zhu, J. Wang, Z. Li, X. Su, C. Niu, Appl. Clay Sci. **105**, 243 (2015)
38. M.R. Belkhedkar, AU Ubale, J. Saudi Chem. Soc. doi:10.1016/j.jscs.2014.11.004
39. F. Ohashi, A. Oya, J. Mater. Sci. **27**, 5027 (1992)
40. J. Joo, S.G. Kwon, T. Yu et al., J. Phys. Chem. B **109**, 15297 (2005)